Optimizing Age of Information in Random-Access Poisson Networks

Xinghua Sun, *Member, IEEE*, Fangming Zhao, Howard H. Yang, *Member, IEEE*, Wen Zhan, *Member, IEEE*, Xijun Wang, *Member, IEEE*, and Tony Q. S. Quek, *Fellow, IEEE*

***Abstract*—Timeliness is an emerging requirement for many Internet of Things (IoT) applications. In IoT networks with a large number of nodes, severe interference may incur that leads to Age-of-Information (AoI) degradation. It is, therefore, important to study how to optimize the AoI performance. This article focuses on the AoI minimization in random-access Poisson networks. By considering the spatiotemporal interactions amongst the transmitters, an expression of the peak AoI is derived, based on which the optimal peak AoI and the corresponding optimal packet arrival rate and channel access probability are further characterized. The analysis shows that when the channel access probability (resp., the packet arrival rate) is given, the optimal packet arrival rate (resp., the optimal channel access probability) is equal to one when nodes are sparsely deployed, and decreases as the node deployment density increases. With a joint tuning of these two system parameters, the optimal channel access probability always equals one. Moreover, with the sole tuning of the channel access probability, the optimal peak AoI is improved with a smaller packet arrival rate only when the node deployment density is high. In contrast, a higher channel access probability always improves peak AoI performance when the packet arrival rate is solely tuned. The analysis in this article sheds important light on freshness-aware design for large-scale networks.**

***Index Terms*—Age of Information (AoI), queuing theory, random access, stochastic geometry.**

Manuscript received March 14, 2021; revised July 3, 2021; accepted September 14, 2021. Date of publication September 27, 2021; date of current version April 25, 2022. The work of Xinghua Sun was supported in part by the Key-Area Research and Development Program of Guangdong Province under Grant 2020B0101120003, and in part by the Guangdong Basic and Applied Basic Research Foundation under Grant 2019A1515011906. The work of Wen Zhan was supported in part by the National Natural Science Foundation of China under Grant 62001524, and in part by the Science, Technology, and Innovation Commission of Shenzhen Municipality under Grant 2021A04. The work of Xijun Wang was supported by the Guangdong Basic and Applied Basic Research Foundation under Grant 2021A1515012631. The work of Tony Q. S. Quek was supported in part by the National Research Foundation, Singapore; in part by the Infocomm Media Development Authority under its Future Communications Research and Development Programme; and in part by MOE ARF Tier 2 under Grant T2EP20120-0006. *(Corresponding author: Wen Zhan.)*

Xinghua Sun, Fangming Zhao, and Wen Zhan are with the School of Electronics and Communication Engineering, Shenzhen Campus of Sun Yat-sen University, Shenzhen 518107, China (e-mail: sunxinghua@mail.sysu.edu.cn; zhaofm@mail2.sysu.edu.cn; zhanw6@mail.sysu.edu.cn).

Howard H. Yang is with the Zhejiang University/University of Illinois at Urbana–Champaign Institute, Zhejiang University, Haining 314400, China, also with the College of Information Science and Electronic Engineering, Zhejiang University, Hangzhou 310007, China, and also with the Department of Electrical and Computer Engineering, University of Illinois at Urbana–Champaign, Champaign, IL 61820 USA (e-mail: haoyang@intl.zju.edu.cn).

Xijun Wang is with the School of Electronics and Information Technology, Sun Yat-sen University, Guangzhou 510006, China (e-mail: wangxijun@mail.sysu.edu.cn).

Tony Q. S. Quek is with the Information System Technology and Design Pillar, Singapore University of Technology and Design, Singapore (e-mail: tonyquek@sutd.edu.sg).

Digital Object Identifier 10.1109/JIOT.2021.3115780

I. INTRODUCTION

THE INTERNET OF THINGS (IoT) network is scheduled to make our physical surroundings accessible by placing sensors on everything in the world and converting the physical information into a digital format. The applications of IoT span numerous verticals, including transportation, environmental detection, and energy scheduling [1], [2]. In such applications, timely message delivery is of necessity. For example, for intelligent vehicles, real-time updates of road information are crucial for safe driving, and in environmental detection, updating environmental information on time is beneficial to the prediction, as well as preparation, for the occurrence of natural disasters. Since an outdated message would become useless, timeliness is one of the critical objectives in the IoT network.

To assess the timeliness of delivered messages, a novel performance metric named the *Age of Information* (AoI) has been put forward in [3] and [4]. Aiming to design systems that can provide fresh information, extensive studies have been conducted to characterize the AoI on the basis of queuing theory. For instance, the AoI was minimized for first-come–first-served (FCFS) M/M/1, M/D/1, and D/M/1 queues in [3]. Multiple sources were considered in [4] for the FCFS M/M/1 queue. In [5], the AoI in M/M/1/1 queue and M/M/1/2 queue with both FCFS and LCFS was characterized by considering a finite buffer capacity. The effects of the buffer capacity, packet age deadline, and preemption on the average AoI were further studied in [6].

However, these studies only focused on a point-to-point communication scenario. In practice, IoT networks generally consist of a large number of nodes that intend to communicate with their destinations via spectrum, which usually constitutes a multiple access network. Due to the broadcast nature of wireless medium, transmissions of nodes will affect each other via the interference they generated. The characterization of AoI under such a setting has attracted a variety of studies recently [7]–[16].

Specifically, the AoI was minimized in [7] and [8] by scheduling a group of links that are active at the same time and limiting the interference to an acceptable level. Various scheduling policies, including Greedy policy, stationary randomized policy, Max-Weight policy, and Whittle's Index policy were proposed in [9] to minimize the AoI for periodic packet arrivals. In addition, the AoI performance under stationary randomized policy and Max-Weight policy was analyzed for Bernoulli packet arrivals [10]. Considering both status sampling and updating process, a novel scheme was designed to optimize the average AoI performance in [11]. Despite the promise of improving the AoI performance, the overhead of centralized scheduling may be too hefty to be affordable for IoT networks with massive connectivity. In that respect, decentralized schemes were also studied from the perspective of AoI optimization. In particular, the effectiveness of slotted ALOHA on minimizing AoI was studied in [12], where each node initializes a channel access attempt at each time slot with a certain probability. A threshold-based age-dependent random-access protocol was proposed in [13] and [14], where each node accesses the channel only when its instantaneous AoI exceeds a predetermined threshold. A distributed transmission policy was proposed in [15] based on the age gain which is the reduction of instantaneous AoI when packets are successfully delivered. An index-prioritized random-access scheme was proposed in [16], where nodes access the radio channel according to their indices that reflect the urgency of update.

The classic collision model was adopted in these studies, where one node can successfully access the channel if and only if there are no other concurrent transmissions. Albeit significant advances have been achieved, these works did not take into account the key effects of physical attributes in wireless systems, such as fading, path loss, and interference. Stochastic geometry on the other hand provides an elegant way of capturing macroscopic properties of such networks by averaging over all potential geographical patterns of the nodes, which can help to account for sources of uncertainties, such as co-channel interference and channel fading. Therefore, this tool has been widely adopted to evaluate the performance of various types of wireless networks [17], [18].

Recently, there have been studies of the AoI performance in large-scale networks by combining queuing theory and stochastic geometry [19]–[25]. In particular, the lower and upper bounds of the average AoI for the Poisson bipolar network were characterized in [19] via the introduction of two auxiliary systems. Based on a dominant system where every transmitter sends out packets in every time slot, [20] devised a locally adaptive channel access scheme for reducing the peak AoI. In these studies, the interference was decoupled from the queue status, i.e., whether the queue is empty or not. To characterize the spatiotemporal interactions of queues, a framework was provided in [21] that captures the peak AoI for large-scale IoT networks with time-triggered (TT) and event-triggered (ET) traffic. The effects of network parameters were further studied in [22] and [23] on the AoI performance in the scenario of random-access networks. However, nonlinear equations have to be solved to calculate the AoI, making it hard to obtain the explicit expressions of network setting for performance optimization. The spatial moments of the mean AoI of the status update links were characterized in [24] and [25] based on the moments of the conditional successful probability.

These studies focused on a static network topology, i.e., the point process pattern is realized at the beginning of time and keeps unchanged after that, leaving the network scenario with mobility largely unexplored. In practical scenarios, devices in some IoT applications may move fast, e.g., smart transportation in the V2V network and UAV nodes, which leads to a dynamic network topology. Yet, how to evaluate and optimize the AoI performance in such a dynamic case remains largely unknown in the existing literature. Therefore, we aim to address this open issue in this article.

In particular, we consider a Poisson bipolar network where each transmitter updates information packets according to an independent Bernoulli process. Similar to that in [5] and [22], we adopt a unit-size buffer at the transmitter side which avoids the long waiting time caused by the accumulation of data packets in the buffer. To reduce the overhead of centralized scheduling, each transmitter employs an ALOHA random-access protocol, i.e., each transmitter accesses the channel with a certain probability at each time slot. The successful transmission of packets depends on the signal-to-interference-plus-noise ratio (SINR) value at the receiver side. Because of the interference, the buffer states of the transmitters are coupled with each other.

By leveraging tools from stochastic geometry and queuing theory, we derive a fixed-point equation of the probability of successful transmission of each transmitter by taking into account the coupling effect. Based on the probability of successful transmission, an analytical expression for the peak AoI is obtained, which is a function of the packet arrival rate and the channel access probability. Using this expression, we find that when the node deployment density is small, the AoI performance can be always improved by choosing a large packet arrival rate or channel access probability. When the node deployment density becomes large, a very high packet arrival rate or channel access probability can in turn deteriorate the AoI performance owing to the severe interference caused by the simultaneous transmissions.

The peak AoI is further optimized by tuning the channel access probability for a given packet arrival rate and by tuning the packet arrival rate for a given channel access probability, respectively. It is found that when the packet arrival rate is optimally tuned, a higher channel access probability always leads to better peak AoI performance, but when the channel access probability is optimally tuned, the peak AoI can be benefited with a smaller packet arrival rate only when the node deployment density is high. We then study how to minimize the peak AoI by jointly tuning the packet arrival rate and the channel access probability, and find that the optimal channel access probability is always set to be one. This indicates that to reduce the waiting time in each transmitters' buffer, each packet should be transmitted as soon as possible. Yet, the packet arrival rate, i.e., the information update frequency, should be lower so as to alleviate the channel contention. For all three cases, i.e., tuning the channel access probability, tuning the packet arrival rate, and joint tuning, the optimal peak AoI grows linearly as the node deployment density increases, which is in sharp contrast to an exponential growth when the system parameters are not properly tuned. It indicates that the

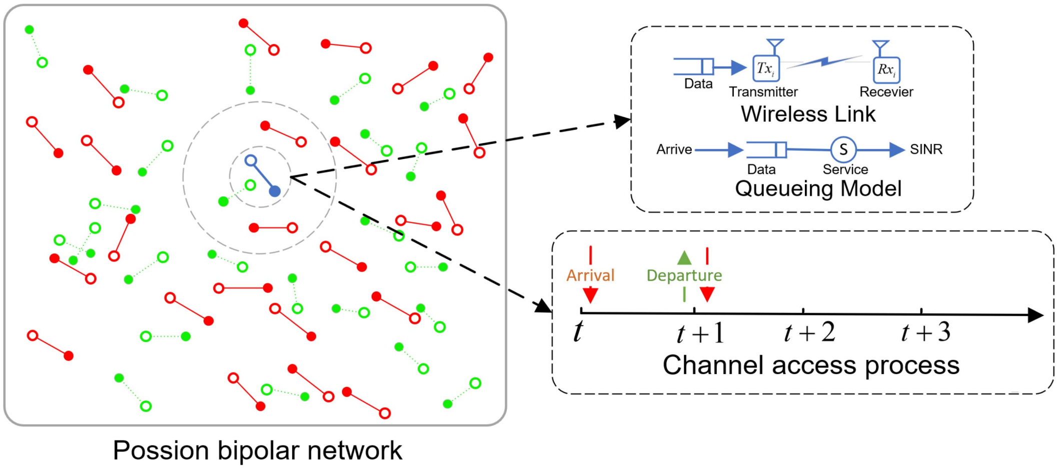

Fig. 1. Snapshot of Poisson bipolar network in consideration. The up-right figure illustrates the queueing model of a generic transmitter. The down-right figure illustrates the channel access process.

TABLE I
KEY NOTATIONS

Notations	Definition	Notations	Definition
λ	Node deployment density	A_p	Peak AoI
R	Distance of each transmitter-receiver pairs	$A_p^{q=q_\xi^*}$	Optimal Peak AoI (Fixed ξ)
ξ	Packet arrival rate	q_ξ^*	Optimal channel access probability (Fixed ξ)
q	Channel access probability	$A_p^{\xi=\xi_q^*}$	Optimal Peak AoI (Fixed q)
α	Path-loss fading coefficient	ξ_q^*	Optimal Packet arrival rate (Fixed q)
γ	SNR	A_p^*	Optimal Peak AoI (Joint optimization)
θ	Decoding SINR threshold	q^*	Optimal channel access probability
p	Probability of successful transmission	ξ^*	Optimal packet arrival rate

analysis in this article provides an important inspiration for the freshness-aware design for large-scale networks.

The remainder of this article is organized as follows. Section II presents the system model and preliminary analysis. Section III shows the derivation and analysis of the probability of successful transmission. In Section IV, the peak AoI is derived and optimized by tuning system parameters, including the channel access probability and the packet arrival rate. Section V presents the simulation results of the above analysis. Finally, Section VI summarizes the work and draws final conclusion.

II. System Model and Preliminary Analysis

Let us consider a Poisson bipolar network,[1] where transmitters are scattered according to a homogeneous Poisson point process (PPP) of density λ. The main notations used throughout this article are summarized in Table I. As Fig. 1 illustrates, each transmitter is paired with a receiver that is situated in distance R and oriented at a random direction. In this network, the time is slotted into equal-length intervals and the transmission of each packet lasts for one slot.

The packets arrive at each transmitter following independent Bernoulli processes[2] of rate ξ. We assume every transmitter is equipped with a unit-size buffer and hence a newly incoming packet will be dropped if an elder packet is in its service. At the beginning of each time slot, transmitters with nonempty buffers will access the channel with a fixed probability q. Similar to [27], we assume a high mobility random walk model.[3] To better illustrate the channel access process of each transmitter, let us define two parameters ϵ and ϵ', where $\epsilon < \epsilon' \ll 1$: 1) at $t + \epsilon$, the position of each link is shifted according to the high mobility random walk model; 2) at $t+\epsilon'$,

[1]A Poisson bipolar network consists of a PPP of transmitters $\{x_i\} \subset \mathbb{R}^2$ and a set of receivers $\{y_i\}$ at a fixed distance and uniformly randomly chosen orientation from their transmitters. By the displacement theorem, the point process of receivers $\{y_i\}$ is itself a PPP. So the Poisson bipolar network consists of two dependent PPPs, namely, a transmitter PPP and a receiver PPP [26].

[2]Note that the analytical methodology in this article can be applied to other packet arrival patterns such as periodic arrivals. In general, the offered load of each transmitter's queue is not solely determined by the mean packet arrival rate, but the nature of the packet arrival process. Therefore, the analysis of the optimal AoI performance should be done case by case.

[3]At each time slot, each node is displaced from its initial position $x \in \mathbb{R}$ to a new position $y \in \mathbb{R}$. In particular, the high mobility random walk case features a small parameter δ and consists in adding the random variable D/δ to x to get the new position, which leads to an independence between Φ (the initial p.p.) and Φ' (the displacement p.p.), when $\delta \to 0$ [26]. The destination moves accordingly, that is, the distance from the source remains constant and the direction is random.

a new packet arrives with probability ξ; 3) at $t+1-\epsilon'$, each transmitter that has one packet in its buffer accesses the radio channel with probability q; 4) if the transmission is successful, then the packet departs at $t+1-\epsilon$; otherwise, the packet remains in the queue and will be sent out until success.

A. Signal-to-Interference-Plus-Noise Ratio

In this article, we consider the radio frequency is globally reused, i.e., all the nodes utilize the same spectrum for packet delivery. Moreover, each transmitter employs a universally unified transmit power and thus has an equal mean received SNR γ at the receiver. As such, for a generic transmitter i, its received SINR at time slot t is given by

$$\mathrm{SINR}_i(t) = \frac{h_{ii}(t)R^{-\alpha}}{\sum_{j\neq i} h_{ij}(t)e_j(t)\mathbf{1}(Q_j(t)>0)d_{ij}(t)^{-\alpha}+\gamma^{-1}} \quad (1)$$

where $h_{ij}(t)$ represents the small-scale fading coefficient between transmitter j and receiver i, which is assumed to be exponentially distributed with unit mean and varies i.i.d. across space and time, d_{ij} is the distance between transmitter j and destination i, and $e_j(t)$ is a binary function, where $e_j(t)=1$ denotes that transmitter j initiates the packet transmission at slot t, and $e_j(t)=0$ otherwise. $Q_j(t)$ is the queue length of transmitter j at slot t. Thus, $\mathbf{1}(Q_j(t)>0)=1$ indicates that transmitter j has a nonempty buffer at time slot t, and $\mathbf{1}(Q_j(t)>0)=0$ otherwise. The parameter α is the path-loss exponent. In this work, we consider a packet is successfully delivered if the received SINR exceeds a decoding threshold θ. Therefore, the corresponding probability of successful transmission for node i can be written as

$$p_i(t) = \mathbb{P}(\mathrm{SINR}_i(t)>\theta). \quad (2)$$

With the high mobility random walk model for the positions of transmitters, the received $\mathrm{SINR}_i(t)$ of each transmitter i, $i\in\mathbb{N}$, can be considered as i.i.d. across time t, which results in independent channel conditions for each time slot. By symmetry, the probability of successful transmission is also identical across all the transmitters. To that end, we drop the indices i and t in (2) and denote p as the probability of successful transmission. Then, the dynamics of packet transmissions over each wireless link can be regarded as a Geo/Geo/1/1 queue with the service rate qp.

B. Performance Metric

In this article, we focus on the performance metric of AoI, which captures the timeliness of information delivered at the receiver side. In Fig. 2, we depict the evolution of AoI $A(t)$ over time for a Geo/Geo/1/1 queue, where t_k denotes the time slot in which the kth packet arrived, t_k' denotes the time slot in which the kth packet is successfully transmitted, and t_k^* denotes the time slot in which the kth packet is dropped. From this figure, we can see that the AoI $A(t)$ increases linearly over time and plummets at time slots $t_1', t_2', t_3', \ldots, t_n'$, where packets are successfully transmitted. Notably, during the period between t_2 and t_2', there is a packet arrivals at slot t^* but is immediately discarded because the buffer can accommodate only one packet. Formally, the progress of such a process can be written as

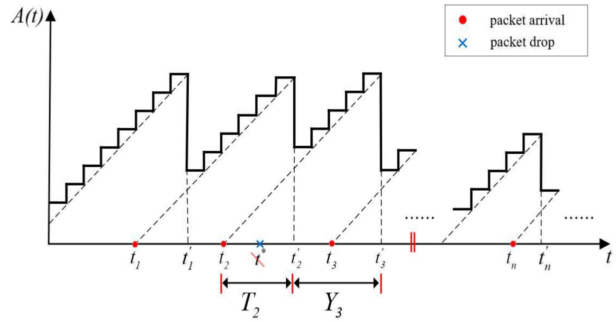

Fig. 2. Example of the AoI evolution over time.

$$A(t+1) = \begin{cases} A(t)+1 & \text{transmission failure} \\ t-t_k+1 & \text{transmission successful.} \end{cases} \quad (3)$$

In this article, we focus on the peak AoI, denoted as A_p, which is defined as the time average of age values at time instants when there is packet transmitted successfully. Such a metric is given by [28]

$$A_p = \lim_{T\to\infty} \sup \frac{\sum_{t=1}^{t=T} A(t)\mathbf{1}\{A(t+1)\leq A(t)\}}{\sum_{t=1}^{t=T}\mathbf{1}\{A(t+1)\leq A(t)\}}. \quad (4)$$

III. Probability of Successful Transmission

The AoI performance is dependent on the probability of successful transmission of each update packet. This section is then devoted to the characterization of the probability of successful transmission. First, the following lemma shows that the probability of successful transmission can be written in the form of a fixed-point equation.

Lemma 1: The probability of successful transmission of a generic transmitter can be obtained as

$$p = \exp\left\{-\lambda c R^2 \frac{q\xi}{\xi+pq(1-\xi)} - \theta R^{\alpha}\gamma^{-1}\right\} \quad (5)$$

where $c=\pi\theta^{(2/\alpha)}/\operatorname{sinc}(2/\alpha)$.

Proof: See Appendix A. ■

Remark 1: With the mobility model, the correlation of the received SINR of each transmitter becomes i.i.d. across time. As a result, the spatiotemproal interaction among the queues can be captured by Lemma 1. If nodes do not move, then the queueing status and active state vary largely from link to link [23]. For this case, the probability of successful transmission of each transmitter would differ from each other and cannot be characterized based on Lemma 1.

Due to similar reasons, the analysis cannot apply to nonhomogeneous PPP. In the nonhomogeneous PPP case, nodes are distributed unevenly, and then one receiver might experience severe interference when it locates at a densely populated area. In this case, each pair would have a distinct probability of successful transmission.

Lemma 1 indicates that the probability of successful transmission p is determined by the channel access probability q, the packet arrival rate ξ, the node deployment density λ, and the TX–RX distance R. The following result further characterizes the distribution of roots of (5).

Theorem 1: The fixed-point equation of the probability of successful transmission (5) has three nonzero roots $0 < p_A \le p_S \le p_L < 1$ if $(4/q) < \lambda c R^2 < ((1-\xi)q + \xi)^2/[q^2\xi(1-\xi)]$ and $\xi_l < \xi < \xi_h$, where ξ_l and ξ_h are, respectively, given as follows:

$$\xi_l = \frac{q}{q + \frac{\frac{q\lambda c R^2}{2} - 1 - q\lambda c R^2\sqrt{\frac{1}{4} - \frac{1}{q\lambda c R^2}}}{\exp\left\{-\theta R^\alpha \gamma^{-1} - \frac{1}{\frac{1}{2} - \sqrt{\frac{1}{4} - \frac{1}{q\lambda c R^2}}}\right\}}} \tag{6}$$

and

$$\xi_h = \frac{q}{q + \frac{\frac{q\lambda c R^2}{2} - 1 + q\lambda c R^2\sqrt{\frac{1}{4} - \frac{1}{q\lambda c R^2}}}{\exp\left\{-\theta R^\alpha \gamma^{-1} - \frac{1}{\frac{1}{2} + \sqrt{\frac{1}{4} - \frac{1}{q\lambda c R^2}}}\right\}}} \tag{7}$$

otherwise, (5) has only one nonzero root $0 < p_L \le 1$.

Proof: See Appendix B. ■

According to the approximate trajectory analysis [29], not all roots in (5) are steady-state points. More precisely situations are as follows.

1) If (5) has only one nonzero root p_L, then p_L is a steady-state point.
2) If (5) has three nonzero roots $0 < p_A \le p_S \le p_L \le 1$, then only p_L and p_A are steady-state points.

Corollary 1 further summarizes the properties of the steady-state points with regard to the system parameters.

Corollary 1: The steady-state points p_A and p_L are monotonic decreasing functions of the node deployment density λ, the packet arrival rate ξ, and the channel access probability q,

Proof: See Appendix C. ■

It is intuitively clear that with dense node deployment, a high packet arrival rate, and a large channel access probability, the channel contention becomes intensive, which deteriorates the probability of successful transmission.

IV. Peak Age-of-Information Optimization

In this section, we first derive an expression of the peak AoI in the random-access Poisson network. Based on that we then optimize the peak AoI by tuning the channel access probability q and the packet arrival rate ξ.

According to Fig. 2, the kth packet's service time can be expressed as $T_k = t'_k - t_k$, and the interdeparture time between the $(k-1)$th packet and kth packet can be written as $Y_k = t'_k - t'_{k-1}$. Then, the peak AoI can be expressed as $A_p = E[T_k] + E[Y_k]$. Lemma 2 gives the explicit expression of the peak AoI.

Lemma 2: Under the Geo/Geo/1/1 queue assumption with FCFS discipline, the peak AoI A_p can be given by

$$A_p = E[T_{k-1}] + E[Y_k] = \frac{1}{\xi} + \frac{2}{qp} - 1. \tag{8}$$

Proof: See Appendix D. ■

Lemma 2 shows that the peak AoI A_p is affected by the channel access probability q and the packet arrival rate ξ. Consequently, it is of great importance to explore how to properly tune the channel access probability q and the packet arrival rate ξ so as to minimize the peak AoI A_p, we then establish the following optimization problem:

$$\begin{aligned} A_p^* = \; & \min_{\{q,\xi\}} \quad A_p \\ & \text{s.t.} \quad q \in (0, 1], \\ & \qquad\;\; \xi \in (0, 1]. \end{aligned} \tag{9}$$

The optimization problem in (9) can be decomposed into two suboptimization problems: 1) optimal tuning of channel access probability q for a fixed ξ and 2) optimal tuning of the packet arrival rate ξ for a fixed q. In the following, we will first look into those two suboptimization problems and then solve the joint tuning problem in (9). The reason is twofold.

First, joint tuning of channel access probability and the packet arrival rate might be infeasible in some practical scenarios. For the channel access probability, as we will show in Theorem 2, the optimal channel access probability $q^* = 1$ when node deployment density λ or the TX–RX distance R is small. Yet, with $q^* = 1$, devices would transmit packets in every time slot if it has packets in its buffer, which drains the battery out rapidly and does not serve the interest of IoT applications, where sensors are battery-limited. In this case, the system may set a small value of the channel access probability q to reduce the power consumption of air interface, which makes q a fixed parameter and unable to be tuned. The packet arrival rate is usually determined by the applications and might be fixed if the traffic shaping is not applied. For instance, for the power grid state reporting in smart grid, the mean reporting period is set to be every 15 min [30]. For these scenarios where a joint tuning is not allowed or not appropriate, separate tuning becomes vital for the AoI performance.

Second, from the perspective of solving the optimization problem, we have

$$A_p^* = \min_{\{q,\xi\}} A_p = \min_q A_p^{\xi=\xi_q^*} = \min_\xi A_p^{q=q_\xi^*}. \tag{10}$$

It is clear that to solve the jointly tuning optimization problem, we can first solve the separately tuning optimization problem.

A. Optimal Tuning of Channel Access Probability q

The following theorem presents the optimal channel access probability q_ξ^* that minimizes the peak AoI A_p, i.e., $A_p^{q=q_\xi^*} = \min_q A_p$.

Theorem 2: Given a packet arrival rate ξ, the optimal peak AoI $A_p^{q=q_\xi^*}$ is given by

$$A_p^{q=q_\xi^*} = \begin{cases} 2\lambda c R^2 \exp\left\{\theta R^\alpha \gamma^{-1} + 1\right\} - \frac{1}{\xi} + 1, & \text{if } \lambda c R^2 > 1 + \frac{p_*(1-\xi)}{\xi} \\ \frac{1}{\xi} + \frac{2}{p^*} - 1, & \text{otherwise} \end{cases} \tag{11}$$

which is achieved when the channel access probability q is set to be

$$q_\xi^* = \begin{cases} \frac{1}{\lambda c R^2 - \frac{1-\xi}{\xi}\exp\left\{-\theta R^\alpha \gamma^{-1} - 1\right\}}, & \text{if } \lambda c R^2 > 1 + \frac{p_*(1-\xi)}{\xi} \\ 1, & \text{otherwise} \end{cases} \tag{12}$$

where p_* is the nonzero root of the following equation:

$$p_* = \exp\left\{-\lambda c R^2 \frac{\xi}{\xi + p_*(1-\xi)} - \theta R^\alpha \gamma^{-1}\right\}. \tag{13}$$

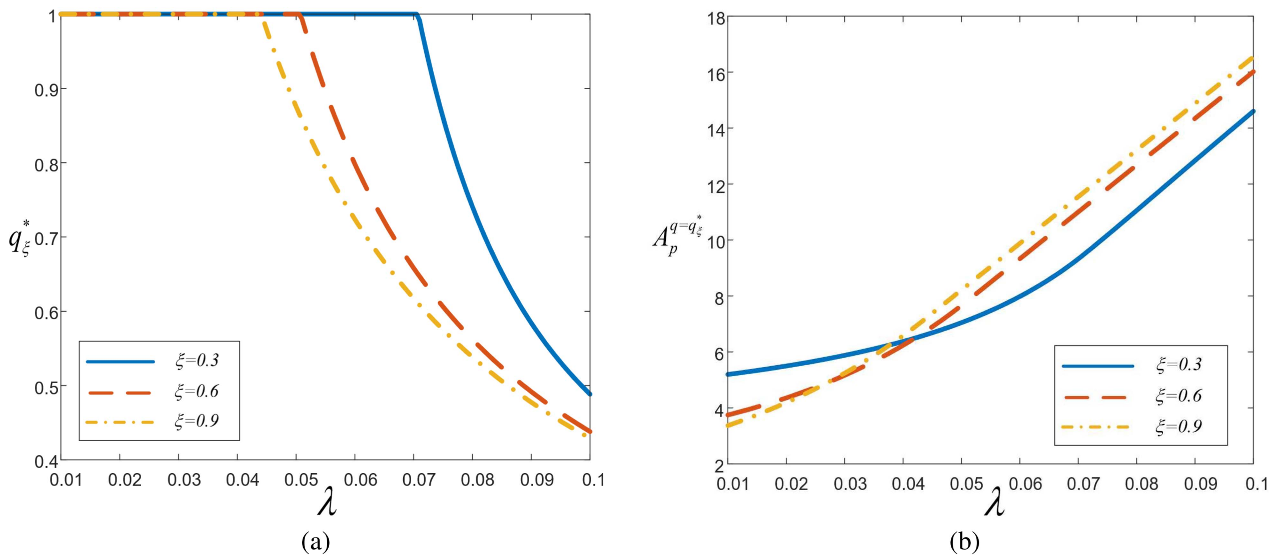

Fig. 3. Optimal channel access probability q_ξ^* and the corresponding peak AoI $A_p^{q=q_\xi^*}$ versus the node deployment density λ. $\alpha = 3$, $\theta = 0.2$, $\gamma = 20$, $R = 3$, and $\xi \in \{0.3, 0.6, 0.9\}$. (a) q_ξ^* versus λ. (b) $A_p^{q=q_\xi^*}$ versus λ.

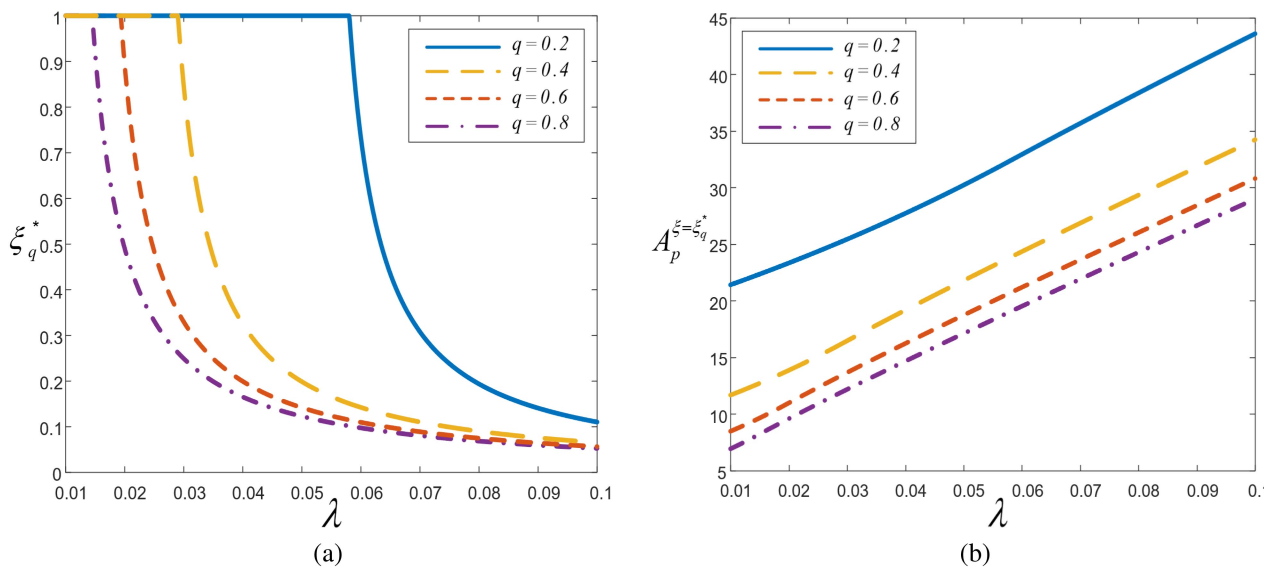

Fig. 4. Optimal packet arrival rate ξ_ξ^* and the corresponding peak AoI $A_p^{\xi=\xi_\xi^*}$ versus the node deployment density λ. $\alpha = 3$, $\theta = 0.5$, $\gamma = 20$, $R = 3$, and $\xi \in \{0.2, 0.4, 0.8\}$. (a) ξ_ξ^* versus λ. (b) $A_p^{\xi=\xi_\xi^*}$ versus λ.

Proof: See Appendix E. ■

Theorem 2 shows that the optimal channel access probability $q_\xi^* = 1$ when $\lambda c R^2 \leq 1 + (p_*(1-\xi)/\xi)$, indicating that in this case, each node would transmit its packet as long as the buffer is nonempty. As the node deployment density λ, the distance between each TX–RX distance R or the decoding threshold θ [equivalently, c according to (5)] grows, we have $q_\xi^* < 1$ due to either mounting channel contention or a lower chance of successful packet decoding.

To take a closer look at Theorem 2, Fig. 3 demonstrates how the optimal channel access probability q_ξ^* and the corresponding the peak AoI $A_p^{q=q_\xi^*}$ vary with the node deployment density λ under different values of the packet arrival rate ξ. It can be seen that when λ is small, e.g., $\lambda = 0.02$, the optimal channel access probability $q_\xi^* = 1$ regardless of the value of the packet arrival rate ξ. Yet, the peak AoI $A_p^{q=q_\xi^*}$ crucially depends on ξ. Intuitively, a smaller node deployment density can reduce the interference among transmitter–receiver pairs, which improves the probability of successful packet transmission. Accordingly, the age performance could be effectively improved with more frequent updates, i.e., a larger packet arrival rate ξ. Therefore, as shown in Fig. 3(b), $A_p^{q=q_\xi^*}$ with $\xi = 0.9$ is lower than those with $\xi = 0.6$ or $\xi = 0.3$ when the node deployment density λ is small.

On the other hand, if the node deployment density λ grows, then to relieve the channel contention, the system should reduce the channel access probability q as well as the packet arrival rate ξ. Thus, we can see q_ξ^* decreases with λ and the descent position, i.e., the starting point that $q_\xi^* < 1$, is positively correlated with the packet arrival rate ξ. In this case, it is interesting to observe that the peak AoI $A_p^{q=q_\xi^*}$ can be benefited with a lower packet arrival rate ξ, which is in sharp contrast to the case where the node deployment density λ is small. Accordingly, as the node deployment density λ increases, a cross point can be observed in Fig. 3(b).

B. Optimal Tuning of Packet Arrival Rate ξ

The following theorem presents the optimal packet arrival rate ξ_q^* that minimizes the peak AoI A_p, i.e., $A_p^{\xi=\xi_q^*} = \min_\xi A_p$.

Theorem 3: Given a channel access probability q, the optimal peak AoI $A_p^{\xi=\xi_q^*}$ is given by

$$A_p^{\xi=\xi_q^*} = \begin{cases} \dfrac{q\lambda c R^2(\psi+1)+2}{2q\exp\left\{-\frac{2}{\psi+1}-\theta R^\alpha\gamma^{-1}\right\}}, & \text{if } \lambda c R^2 > \frac{1}{2q} \\ \frac{2}{q}\exp\left\{\lambda c R^2 q + \theta R^\alpha \gamma^{-1}\right\}, & \text{otherwise} \end{cases} \quad (14)$$

which is achieved when the packet arrival rate ξ is set to be

$$\xi_q^* = \begin{cases} \dfrac{2q\exp\left\{-\frac{2}{\psi+1}-\theta R^\alpha\gamma^{-1}\right\}}{q\lambda c R^2(\psi+1)+2q\exp\left\{-\frac{2}{\psi+1}-\theta R^\alpha\gamma^{-1}\right\}-2}, & \text{if } \lambda c R^2 > \frac{1}{2q} \\ 1, & \text{otherwise} \end{cases} \quad (15)$$

where $\psi = \sqrt{(1+4/(q\lambda c R^2))}$.

Proof: See Appendix F. ■

Theorem 3 reveals that the optimal packet arrival rate $\xi_q^* = 1$ when $\lambda c R^2 \le (1/2q)$, indicating that in this case, to minimize the peak AoI, new packets shall be updated as frequent as possible. Similar to Theorem 2, as λ, R, or c grows, due to mounting channel contention or a lower probability of successful transmission, the optimal packet arrival rate $\xi_q^* < 1$.

Fig. 4 demonstrates how the optimal packet arrival rate ξ_q^* and the corresponding the peak AoI $A_p^{\xi=\xi_q^*}$ varies with the node deployment density λ under various value of the channel access probability. Intuitively, as the node deployment density λ increases, to reduce the interference, the system should either reduce the channel access probability q or the packet arrival rate ξ. Accordingly, we can see from Fig. 4(a) that as λ increases, the optimal packet arrival rate ξ_q^* declines, which could be further reduced with a larger channel access probability q. On the other hand, as shown in Fig. 4(b), the corresponding the peak AoI $A_p^{\xi=\xi_q^*}$ grows with the node deployment density λ, which is intuitively clear. Yet, in contrast to that in Fig. 3(b), a larger channel access probability q always leads to a smaller $A_p^{\xi=\xi_q^*}$.

C. Joint Tuning of q and ξ

So far, we have explicitly characterized the optimal tuning of the channel access probability q for given the packet arrival rate ξ, and the optimal tuning of packet arrival rate ξ for given the channel access probability q. In this section, we will study how to jointly tuning of the channel access probability q and the packet arrival rate ξ to further optimize the age performance.

In particular, it is shown in Appendix G that A_p^* is obtained by tuning the channel access probability q to minimize the $A_p^{\xi=\xi_q^*}$. It has been shown in Theorem 3, i.e., a larger channel access probability q always leads to a smaller $A_p^{\xi=\xi_q}$. Therefore, the optimal channel access probability in joint optimization is always set to be one. The following theorem presents the result of joint tuning of the channel access probability q and the packet arrival rate ξ for minimizing the peak AoI A_p, i.e., $A_p^* = \min_{\{q,\xi\}} A_p$.

Theorem 4: The optimal peak AoI $A_p^* = \min_{\{q,\xi\}} A_p$ is given by

$$A_p^* = \begin{cases} \dfrac{\lambda c R^2\left(\sqrt{1+\frac{4}{\lambda c R^2}}+1\right)+2}{2\exp\left\{-\frac{2}{\sqrt{1+\frac{4}{\lambda c R^2}}+1}-\theta R^\alpha\gamma^{-1}\right\}}, & \text{if } \lambda c R^2 > \frac{1}{2} \\ 2\exp\left\{\lambda c R^2 + \theta R^\alpha\gamma^{-1}\right\}, & \text{otherwise} \end{cases} \quad (16)$$

which is achieved when the channel access probability q is set to be

$$q^* = 1 \quad (17)$$

and the packet arrival rate ξ is set to be

$$\xi^* = \begin{cases} \dfrac{2\exp\left\{\frac{-2}{\sqrt{1+\frac{4}{\lambda c R^2}}+1}-\theta R^\alpha\gamma^{-1}\right\}}{\lambda c R^2\left(\sqrt{(1+\frac{4}{\lambda c R^2})}+1\right)+2\exp\left\{\frac{-2}{\sqrt{1+\frac{4}{\lambda c R^2}}+1}-\theta R^\alpha\gamma^{-1}\right\}-2}, & \text{if } \lambda c R^2 > \frac{1}{2} \\ 1, & \text{otherwise.} \end{cases} \quad (18)$$

Proof: See Appendix G. ■

Fig. 5 demonstrates how the optimal channel access probability q^*, the optimal packet arrival rate ξ^* and the corresponding minimum peak AoI A_p^* vary with the node deployment density λ. It is clear from Fig. 5 that the optimal packet arrival rate $\xi^* = 1$ when $\lambda c R^2 \le 1/2$, indicating that in this case, to minimize the peak AoI, packets should arrive at the system as many as possible. Similar to Theorem 2, as λ, R, or c grows, due to mounting channel contention or a lower probability of successful transmission, the optimal packet arrival rate $\xi^* < 1$. In such a joint optimization, it is interesting to see that we always have $q^* = 1$ whatever the value of λ is. Intuitively, as λ increases, to reduce the channel contention, the system should decrease both q and ξ. Yet, the shorter a period the packet stays in the buffer, the lower AoI will be when it is updated. Accordingly, the system keeps the optimal channel access probability $q^* = 1$ while reduces the packet arrival rate ξ^* only.

V. Simulation Results and Discussion

In this section, we provide simulation results to validate the analysis and further shed light on AoI minimum network designs. Specifically, in the beginning of each simulation run, the locations of transmitter–receiver pairs are realized over a 200×200 m^2 square area according to independent PPPs and place the typical link where the receiver is located at the

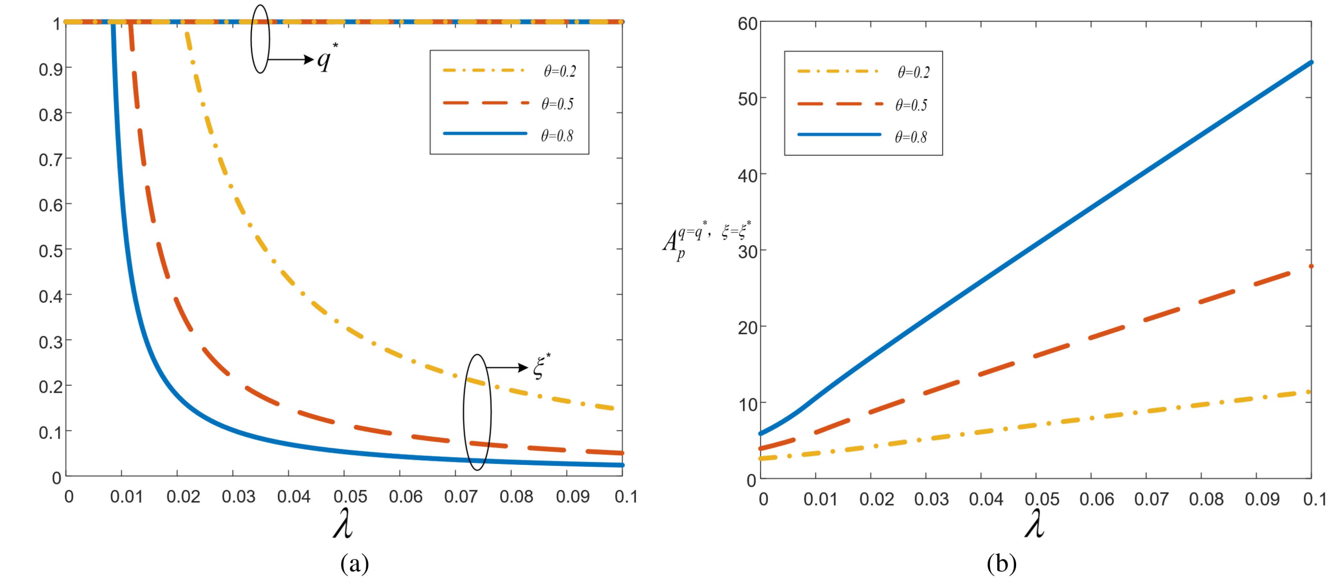

Fig. 5. Optimal channel access probability q^*, the packet arrival rate ξ^*, and the corresponding peak AoI $A_p^{\xi=\xi^*,q=q^*}$ versus the node deployment density λ. $\alpha = 3$, $\gamma = 20$, $R = 3$, and $\theta \in \{0.2, 0.5, 0.8\}$. (a) ξ^*, q^* versus λ. (b) $A_p^{\xi=\xi^*,q=q^*}$ versus λ.

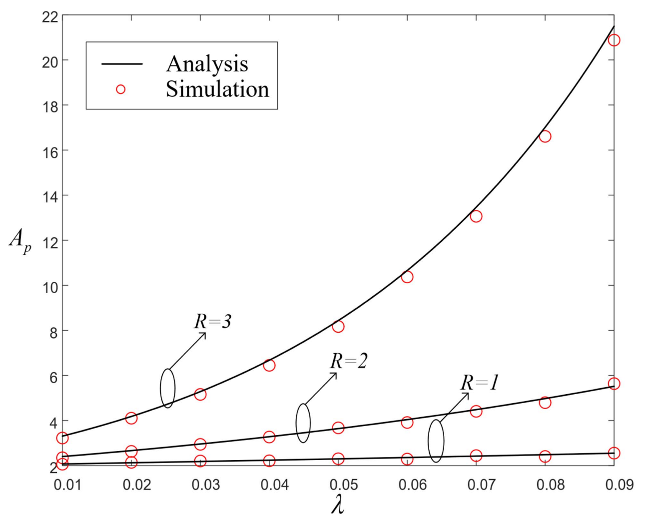

Fig. 6. Peak AoI A_p versus the node deployment density λ. $q = 1$, $\xi = 1$, and $R \in \{1, 2, 3\}$.

TABLE II
SIMULATION PARAMETERS

Notation	Value
System parameters	
TX-RX Distance R	2 m (Fig 8); 3 m
Decoding SINR threshold θ	0.2 (Fig 6); 0.8
Path-loss fading coefficient α	3.0
SNR γ	20
Simulation parameters	
Poisson network deployment area	200*200 m^2
Number of slots in each simulation	10^6

center of the area. In each time slot, the location of each pair is shifted except for the typical link, and each simulation lasts for 10^6 time slots. In each realization, the simulated peak AoI is calculated as the sum of the peak value of AoI curve to the number of successful transmissions of the typical link. The system and simulation parameters are summarized in Table II.

Fig. 6 illustrates how the peak AoI A_p varies with the node deployment density λ under different TX–RX distances. From this figure, we can see that the simulation results match well with the analysis, which verifies the accuracy of Theorem 2. Moreover, following the developed analysis, we know that as the node deployment density goes up, the interference among the wireless link becomes more severe, leading to a smaller probability of successful transmissions that deteriorates the age performance. Accordingly, we can see from Fig. 6 that the peak AoI A_p increases as λ increases. By reducing the TX–RX distance of each pair the SINR can be improved. As Fig. 6 illustrates, when the distance of each pair is reduced to be $R = 1$, the peak AoI A_p becomes less sensitive to the variation of the node deployment density λ.

Fig. 7 depicts the peak AoI A_p as a function of the channel access probability q under various values of the node deployment density λ. It can be seen that when the node deployment density λ is small, A_p monotonically decreases with respect to q and reaches the smallest value when $q = 1$. Note that an increase in the channel access probability has two opposite effects on the peak AoI. On the one side, a larger channel access probability q results in a short waiting time in the buffer which reduces the staleness of the information packet. On the other side, a larger channel access probability q can also incur severe interference due to a high offered loads of each transmitter's queue, leading to a lower probability of successful transmission. As Fig. 7 illustrates, the node deployment density λ determines how these two effects tradeoff with each other. In particular, with a small node deployment density, the interference would not become severe even the channel access

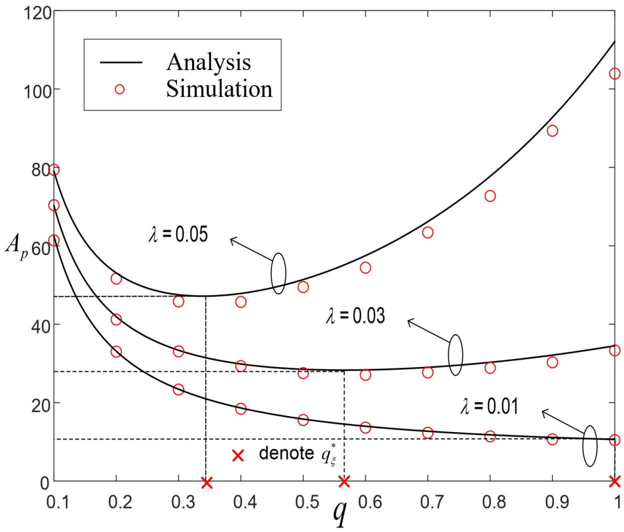

Fig. 7. Peak AoI A_p versus the channel access probability q. $\xi = 1$ and $\lambda \in \{0.01, 0.03, 0.05\}$.

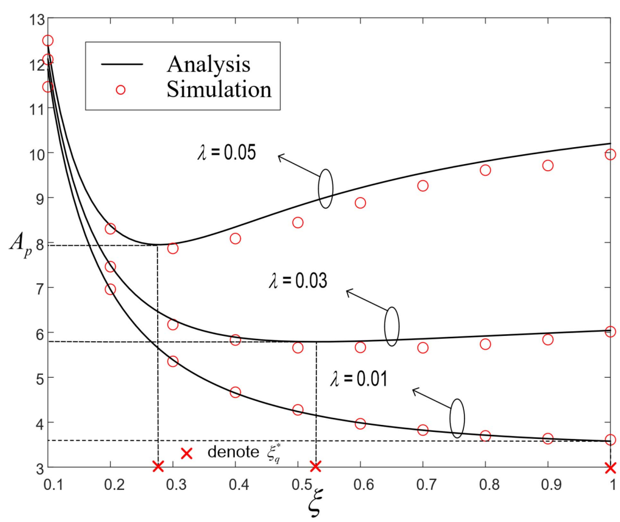

Fig. 8. Peak AoI A_p versus the packet arrival rate ξ. $q = 1$ and $\lambda \in \{0.01, 0.03, 0.05\}$.

probability q is large. With a large λ, on the other hand, the interference can deteriorate the AoI if q is large.

Similar observations can also be seen from Fig. 8, which demonstrates how the peak AoI A_p varies with the packet arrival rate ξ under different values of the node deployment density.

The optimal channel access probability q_ξ^* under a given packet arrival rate ξ and the optimal packet arrival rate ξ_q^* for a given channel access probability q are illustrated in Figs. 7 and 8, respectively. It can be seen that by optimally tuning q and ξ, the peak AoI can be largely reduced. To further investigate the performance gain brought by joint tuning the channel access probability q and the packet arrival rate ξ, Fig. 9 demonstrates how the peak AoI A_p varies with the node deployment density λ in four cases: 1) fixed ξ and q; 2) optimal q with fixed ξ; 3) optimal ξ with fixed q; and 4) joint optimal tuning of q and ξ. We can clearly see that with fixed ξ and q, the peak AoI A_p exponentially increases

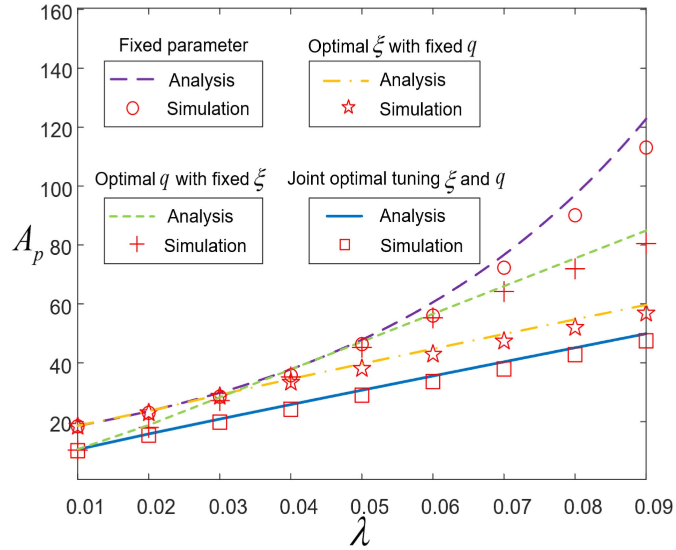

Fig. 9. Optimal peak AoI A_p versus the node deployment density. 1) Fixed parameter: $\xi = 1$ and $q = 0.4$, 2) optimal q with fixed $\xi = 1$, 3) optimal ξ with fixed $q = 0.4$, and 4) joint optimal tuning q and ξ.

with λ. In sharp contrast, with a joint optimal tuning of q and ξ, the peak AoI A_p linearly increases with λ. It implies that the performance gain becomes significant when λ is large.

VI. Conclusion and Future Work

In this article, we conducted an analytical study of optimizing AoI in a random-access network by tuning system parameters such as the channel access probability and the packet arrival rate. Analytical expressions for the optimal peak AoI, as well as the corresponding system parameters, are derived for cases of separately tuning and jointly tuning. In the separately tuning case, when the node deployment density is small, information packets should be generated as frequently as possible, so as to achieve the optimal AoI performance. The same can apply to the optimal channel access probability, where transmitters should access the channel at each time slot. When the node deployment density becomes large, the optimal packet arrival rate and the optimal channel access probability should decrease as the node deployment density increases. In the jointly tuning case, in contrast, the optimal channel access probability is always set to be one and the optimal packet arrival rate shall decrease as the node deployment density increases. For all the cases of separately or jointly tuning of the channel access probability and the packet arrival rate, the optimal peak AoI linearly grows with the node deployment density as opposed to an exponential growth with the fixed channel access probability and the packet arrival rate. It is therefore of crucial importance to properly tune these parameters toward a satisfactory AoI performance especially in dense networks.

Note that although this article focuses on the optimization of the peak AoI, the average AoI performance can also be characterized based on the analytical approach adopted in this article. It is of practical importance to further perform average AoI performance optimization under the proposed analytical approach. Moreover, in this article, we focus on the homogeneous case where all devices have an identical traffic input rate and channel access probability. The analysis could be extended to heterogeneous scenarios where nodes are divided into several groups according to distinct traffic characteristics. It is conjectured that transmitters could have distinct probabilities of successful transmission for each group, which could be jointly determined by a set of nonlinear equations. The corresponding computational complexity increases rapidly as the number of groups in the network grows, which would nevertheless become intolerably high if the number of groups is large. How to reduce the computational complexity and further optimize the AoI performance deserves future study.

Appendix A
Proof of Lemma 1

Note that according to [31, eqs. (9) and (10)], the probability of successful transmission p is determined by the following equation:

$$p = \exp\{-\lambda c R^2 \rho q - \theta R^{\alpha} \gamma^{-1}\} \tag{19}$$

where $c = [\pi \theta^{\frac{2}{\alpha}}]/[\mathrm{sinc}[2/\alpha]]$ and ρ denotes the offered load of each transmitter. To derive the offered load ρ, let us define the state of each transmitter at time t as the number of packets in the buffer at the beginning of the time slot. As the buffer size of each transmitter is one, the state transition process of each transmitter can be model as a Markov chain with the state space $\mathbf{X} = \{0, 1\}$, where the transition matrix is given by

$$\mathbf{P} = \begin{bmatrix} p_{0,0} & p_{0,1} \\ p_{1,0} & p_{1,1} \end{bmatrix} = \begin{bmatrix} 1-\xi+\xi qp & \xi(1-qp) \\ qp & 1-qp \end{bmatrix} \tag{20}$$

where $p_{i,j}$ is the probability of transiting $i \in \mathbf{X}$ to state $j \in \mathbf{X}$. According to (20), the steady-state distribution can be derived as

$$\begin{cases} \pi_0 = \frac{qp}{\xi+qp-\xi qp} \\ \pi_1 = \frac{\xi-\xi qp}{\xi+qp-\xi qp}. \end{cases} \tag{21}$$

The offered load ρ can then be written as

$$\rho = \frac{r}{qp} \tag{22}$$

where r is the effective packet arrival rate. As one incoming packet would be dropped if it sees a full buffer, the effective packet arrival rate r is given by

$$r = \xi \pi_0 = \frac{\xi qp}{\xi + qp - \xi qp}. \tag{23}$$

By combining (22) and (23), the offered load of each transmitter ρ can be obtained as

$$\rho = \frac{\xi}{\xi + qp - \xi qp}. \tag{24}$$

Finally, (5) can be obtained by substituting (24) into (19).

Appendix B
Proof of Theorem 1

Let

$$f(p) = -\ln p - \frac{M}{N+p} - K \tag{25}$$

where

$$M = \lambda c R^2 \frac{\xi}{1-\xi}, \quad N = \frac{\xi}{q(1-\xi)}, \quad K = \theta R^{\alpha} \gamma^{-1}. \tag{26}$$

Since $f(p) = 0$ is the equivalent change of (5), it can be used to analyze the number of roots for simplicity. The first derivative of $f(p)$ about p can be obtained as $f'(p) = [\phi(p)/p(N+p)^2]$, where

$$\phi(p) = -\left(p + N - \frac{M}{2}\right)^2 + \frac{M^2}{4} - MN. \tag{27}$$

Lemma 3 shows that the number of nonzero roots of $\phi(p) = 0$ for $p \in (0, 1]$ determines the number of nonzero roots of $f(p) = 0$ for $p \in (0, 1]$.

Lemma 3: $f(p) = 0$ has three nonzero roots of $0 < p_A < p_S < p_L < 1$, if and only if $\phi(p) = 0$ has two nonzero roots $0 < p_1' < p_2' < 1$ with $f(p_1') < 0$ and $f(p_2') > 0$; otherwise, $f(p) = 0$ has only one nonzero root $0 < p_L < 1$.

Proof: Because of $\lim_{p\to 0} f(p) > 0, f(1) = -(M/(N+1)) - K < 0$ and $f(p)$ is continuous function, according to the zero-point theorem, $f(p)$ has nonzero root. Moreover, $p(N+p)^2 > 0$ when $p \in (0, 1]$. Thus, the number of nonzero roots of $\phi(p) = 0$ for $p \in (0, 1]$ determines the number of nonzero roots of $f'(p) = 0$ for $p \in (0, 1]$, and we only consider the root of $\phi(p)$ in the following scenarios.

1) Assume that $\phi(p) = 0$ has not nonzero root when $p \in (0, 1]$, then in this case $\phi(p) < 0$ for $p \in (0, 1]$. Thus, $f'(p) < 0$ and $f(p)$ decreases monotonically when $p \in (0, 1]$, so $f(p)$ only has one nonzero root.
2) Assume that $\phi(p) = 0$ has one nonzero root $0 < p' \leq 1$, then, we have the following.
   a) If $\phi(p) = 0$ has two roots when $p \in \mathbb{R}$, and one of them in range $p \in (0, 1)$, we mark the root in (0,1) as p'. So when $p \in (0, p')$, $f(p)$ monotonically decrease and $p \in (p', 1)$, $f(p)$ monotonically increase, and we have $f(1) < 0$, thus $f(p)$ only has one nonzero root.
   b) If $\phi(p) = 0$ has one root when $p \in \mathbb{R}$, and this root in range $p \in (0, 1)$, then $f(p)$ monotonically decrease when $p \in (0, 1)$, so $f(p)$ only has one nonzero root. Combining two cases, when $\phi(p) = 0$ has one nonzero root, $f(p) = 0$ only has one nonzero root.
3) Assume that $\phi(p) = 0$ has two nonzero roots $0 < p_1' < p_2' < 1$, then we have the following.
   a) If $p_2' = 1$, then $\phi(p) < 0$ for $p \in (0, p_1')$ and $\phi(p) > 0$ for $p \in (p_1', 1)$. Consequently, $f'(p) < 0$ for $p \in (0, p_1')$ and $f'(p) > 0$ for $p \in (p_1', 1)$, indicating that $f(p)$ monotonically decreases for $p \in (0, p_1')$, and increases for $p \in (p_1', 1]$. Since $f(1) < 0$, we can conclude that in this case, $f(p) = 0$ only one nonzero root $0 < p_L < 1$.

b) If $p_2' < 1$, then $\phi(p) < 0$ for $p \in (0, p_1') \cup (p_2', 1)$, and $\phi(p) > 0$ for $p \in (p_1', p_2')$. As a result, $f'(p) < 0$ for $p \in (0, p_1') \cup (p_2', 1)$, and $f'(p) > 0$ for $p \in (p_1', p_2')$, indicating that $f(p)$ monotonically decreases for $p \in (0, p_1') \cup (p_2', 1)$, and increases for $p \in (p_1', p_2')$.Then, we have if $f(p_1') > 0$ or $f(p_2') < 0$, $f(p) = 0$ has one root $0 < p_L \leq 1$; otherwise, $f(p) = 0$ has three nonzero roots $0 < p_A < p_S < p_L \leq 1$ in which $f(p_1') < 0$ and $f(p_2') > 0$. ■

Lemma 4 further concludes the specific condition for $\phi(p) = 0$ has two nonzero roots $0 < p_1' < p_2' < 1$ with $f(p_1') < 0$ and $f(p_2') > 0$.

Lemma 4: $\phi(p) = 0$ has two nonzero roots $0 < p_1' < p_2' < 1$ with $f(p_1') < 0$ and $f(p_2') > 0$ if and only if $4/q < \lambda c R^2 < ((1-\xi)q + \xi)^2/[q^2\xi(1-\xi)]$ and $\xi_l < \xi < \xi_h$, where ξ_l and ξ_h are given in (6) and (7), respectively.

Proof: $\phi(p) = 0$ has two nonzero roots, when $\lim_{p\to 0} \phi(p) < 0$, $\phi(1) < 0$ and peak value of $\phi(p)$ is larger than zero, and find that $\phi(p) = 0$ has two nonzero roots p_1' and p_2', if

$$\frac{4}{q} < \lambda c R^2 < \frac{((1-\xi)q+\xi)^2}{q^2\xi(1-\xi)}, \text{and} \quad 0 < q < 1, 0 < \xi < 1 \tag{28}$$

and

$$p_1' = \frac{M}{2} - N - \sqrt{\frac{M^2}{4} - MN} \tag{29}$$

$$p_2' = \frac{M}{2} - N + \sqrt{\frac{M^2}{4} - MN} \tag{30}$$

from $0 < p_1' < p_2' < 1$, we obtain

$$\lambda c R^2 < \frac{((1-\xi)q+\xi)^2}{q^2\xi(1-\xi)} \tag{31}$$

$$\frac{2}{q} < \lambda c R^2 < \frac{2}{q} + \frac{2}{\xi} - 2. \tag{32}$$

So combining (25), (28), (31), and (32) has three nonzero roots $0 < p_A < p_S < p_L < 1$, if

$$\frac{4}{q} < \lambda c R^2 < \min\left\{\frac{((1-\xi)q+\xi)^2}{q^2\xi(1-\xi)}, \frac{2}{q} + \frac{2}{a} - 2\right\} \tag{33}$$

for $0 < q < 1, 0 < \xi < 1$, and

$$f(p_1') = -\frac{M}{\frac{M}{2} - \sqrt{\frac{M^2}{4} - MN}} - \ln\left(\frac{M}{2} - N - \sqrt{\frac{M^2}{4} - MN}\right) - \theta R^\alpha \gamma^{-1} < 0 \tag{34}$$

and

$$f(p_2') = -\frac{M}{\frac{M}{2} + \sqrt{\frac{M^2}{4} - MN}} - \ln\left(\frac{M}{2} - N + \sqrt{\frac{M^2}{4} - MN}\right) - \theta R^\alpha \gamma^{-1} > 0 \tag{35}$$

where $M = \lambda c R^2(\xi/1-\xi)$, $N = \xi/q(1-\xi)$. First, we simplify (33), which means $4/q < 2/q + 2/\xi - 2$ and $4/q < ((1-\xi)q+\xi)^2/[q^2\xi(1-\xi)]$. From that we can get $q > \xi/1-\xi$. Then, we prove that $2/q + 2/\xi - 2 > ((1-\xi)q+\xi)^2/[q^2\xi(1-\xi)]$ in this case. We have

$$\frac{2}{q} + \frac{2}{\xi} - 2 - \frac{((1-\xi)q+\xi)^2}{q^2\xi(1-\xi)} = \frac{q^2(1-\xi)^2 - \xi^2}{q^2\xi(1-\xi)} \tag{36}$$

As $q > \xi/(1-\xi)$, we get $\xi < 1-1/(1+q)$. And $q \in (0, 1]$, thus, $\xi \in (0, 0.5]$. Then, we get $q^2(1-\xi)^2 > \xi^2$, and we have $2/q + 2/\xi - 2 - ((1-\xi)q+\xi)^2/[q^2\xi(1-\xi)] > 0$, which means (33) can be written as

$$\frac{4}{q} < \lambda c R^2 < \frac{((1-\xi)q+\xi)^2}{q^2\xi(1-\xi)}. \tag{37}$$

Moreover, by combining (26), (34), and (35), we obtain (6) and (7). ■

Consequently, Theorem 1 can be proved by combining Lemmas 3 and 4.

APPENDIX C
PROOF OF MONOTONY OF p_A AND p_L

According to (5), we have

$$\begin{aligned}\frac{\partial p}{\partial \xi} &= \frac{\lambda c R^2 p^2}{\lambda c R^2 p\xi(1-\xi) - (\frac{\xi}{q} + p(1-\xi))^2} \\ &= \frac{\lambda c R^2 p^2}{\phi(p)} \frac{1}{(1-\xi)^2}\end{aligned} \tag{38}$$

$$\begin{aligned}\frac{\partial p}{\partial q} &= \frac{\lambda c R^2 (\frac{\xi}{q})^2 p}{\lambda c R^2 p\xi(1-\xi) - (\frac{\xi}{q} + p(1-\xi))^2} \\ &= \frac{\lambda c R^2 (\frac{\xi}{q})^2 p}{\phi(p)} \frac{1}{(1-\xi)^2}\end{aligned} \tag{39}$$

$$\begin{aligned}\frac{\partial p}{\partial \lambda} &= \frac{c R^2 \frac{\xi}{q}(\xi + pq(1-\xi))}{\lambda c R^2 p\xi(1-\xi) - (\frac{\xi}{q} + p(1-\xi))^2} \\ &= \frac{c R^2 \frac{\xi}{q}(\xi + pq(1-\xi))}{\phi(p)} \frac{1}{(1-\xi)^2}\end{aligned} \tag{40}$$

where $\phi(p)$ is shown in (27). Then, $\phi(p_A) < 0$ and $\phi(p_L) < 0$ are proved as follows.

1) If $\phi(p) = 0$ has not root for $p \in (0, 1]$, then $\phi(p) < 0$ for $p \in (0, 1]$. In this case, (5) has one-zero root p_L, we then have $\phi(p_L) < 0$ and p_L is a steady-state point according to [29].
2) If $\phi(p) = 0$ has one root for $0 < p_1' \leq 1$, then we have the following.
   a) If $\phi(p) = 0$ has two roots when $p \in \mathbb{R}$, and one of them in range $p \in (0, 1]$, then $\phi(p) < 0$ for $p \in (0, p_1')$ and $\phi(p) > 0$ for $p \in (p_1', 1)$. Equation (5) has one-zero root p_L, and $p_L < p_1'$, we then have $\phi(p_L) < 0$ and p_L is a steady-state point according to [29].
   b) If $\phi(p) = 0$ has one root when $p \in \mathbb{R}$, and this root in range $p \in (0, 1)$, then $\phi(p) < 0$ for $p \in (0, 1]$. (5) has one-zero root p_L. We then have $\phi(p_L) < 0$ and p_L is a steady-state point according to [29].

3) If $\phi(p) = 0$ has two roots that $0 < p_1' < p_2' < 1$, two scenarios as follows.
   a) If $p_2' = 1$, then $\phi(p) < 0$ for $p \in (0, p_1')$ and $\phi(p) > 0$ for $p \in (p_1', 1)$, (5) has one root $p_L < p_1'$. We then have $\phi(p_L) < 0$ and p_L is a steady-state point according to [29].
   b) If $p_2' < 1$, then $\phi(p) < 0$ for $p \in (0, p_1') \cup (p_2', 1)$, and $\phi(p) > 0$ for $p \in (p_1', p_2')$. In this case, (5) may has one root $p_L \in (0, p_1') \cup (p_2', 1)$, or three roots $p_A < p_1' < p_S < p_2' < p_L$, among which p_A and p_L are the steady-state point according to [29]. We then have $\phi(p_A) < 0$ and $\phi(p_L) < 0$.

In summary, $\phi(p_A) < 0$ and $\phi(p_L) < 0$ can be proved by combining cases 1)–3). Thus, it can be obtained from (38)–(40) that $(\partial p/\partial \xi) < 0$, $(\partial p/\partial q) < 0$, and $(\partial p/\partial \lambda) < 0$ at both the steady states p_A and p_L.

Appendix D
Proof of Lemma 2

The mathematical expectation of peak AoI can be defined as

$$A_p = E[T_{k-1}] + E[Y_k] \tag{41}$$

where T_{k-1} is service time of the $(k-1)$th packet, Y_k is the interdeparture time, between the $(k-1)$th packet served and the kth packet served. Thus, $E[T_{k-1}]$ can be obtained as

$$E[T_{k-1}] = \frac{1}{qp}. \tag{42}$$

For Y_k, it is a summation of the time interval Y_k^a between the $(k-1)$th packet departure and the kth packet departure, and the time interval Y_k^s between the kth packet arrival and departure, i.e., $Y_k = Y_k^a + Y_k^s$. As Fig. 2 illustrates, the departure of the $(k-1)$th packet and the arrival of the kth packet can occur almost at the same time, but the time interval between the kth packet's arrival and departure costs at least one time slot. Thus, we have, $E[Y_k^a] = (1/\xi) - 1$ and $E[Y_k^s] = (1/qp)$, which leads to

$$E[Y_k] = E[Y_k^a] + E[Y_k^s] = \frac{1}{\xi} - 1 + \frac{1}{qp}. \tag{43}$$

Appendix E
Proof of Theorem 2

According to (5) and (8), we have

$$\begin{aligned}\frac{\partial A_p}{\partial q} &= \frac{-2(p + q\frac{\partial p}{\partial q})}{q^2p^2} \\ &= \frac{2\xi^2}{q^2 p}\left(-\frac{1}{\xi^2} - \frac{\lambda c R^2 \frac{1}{q}}{\lambda c R^2 p\xi(1-\xi) - (\frac{\xi}{q} + p(1-\xi))^2}\right).\end{aligned} \tag{44}$$

We then have

$$\lim_{q\to 0} \frac{\partial A_p}{\partial q} < 0 \tag{45}$$

and

$$\lim_{q\to 1} \frac{\partial A_p}{\partial q} = -\frac{2}{p_*} - \frac{2\lambda c R^2 \xi^2 \frac{1}{p_*}}{\lambda c R^2 p_* \xi(1-\xi) - (\xi + p_*(1-\xi))^2} \tag{46}$$

where p_* is the nonzero root of (13). As $(\partial p/\partial q) < 0$, we have

$$\lambda c R^2 p_* \xi(1-\xi) - (\xi + p_*(1-\xi))^2 < 0. \tag{47}$$

Then, when

$$\lambda c R^2 > \frac{(\xi + p_*(1-\xi))^2}{\xi^2 + p_*\xi(1-\xi)} = 1 + \frac{p_*(1-\xi)}{\xi} \tag{48}$$

we have $\lim_{q\to 1}(\partial A_p/\partial q) > 0$. The peak AoI A_p can then be optimized when $q \in (0, 1)$. By combining $(\partial A_p/\partial q) = 0$ and (5), the optimal channel access probability q can be obtained as

$$q = \frac{1}{\lambda c R^2 - \exp\left\{-\theta R^\alpha \gamma^{-1} - 1\right\} \frac{1-\xi}{\xi}}. \tag{49}$$

The optimal peak AoI can be obtained by substituting (49) into (8).

When $\lambda c R^2 \le 1 + [p_*(1-\xi)/\xi]$, on the other hand, the optimal channel access rate is given by $q = 1$, and the corresponding optimal peak AoI can be obtained by combining $q = 1$ and (8).

Appendix F
Proof of Theorem 3

According to (5) and (8), we have

$$\begin{aligned}\frac{\partial A_p}{\partial \xi} &= -\left(\frac{1}{\xi^2} + \frac{2\frac{\partial p}{\partial \xi}}{qp^2}\right) \\ &= -\frac{1}{\xi^2} - \frac{2\lambda c R^2 \frac{1}{q}}{\lambda c R^2 p\xi(1-\xi) - (\frac{\xi}{q} + p(1-\xi))^2}.\end{aligned} \tag{50}$$

We then have

$$\lim_{\xi\to 0} \frac{\partial A_p}{\partial \xi} < 0 \tag{51}$$

and

$$\lim_{\xi\to 1} \frac{\partial A_p}{\partial \xi} = 2\lambda c R^2 q - 1. \tag{52}$$

When $\lambda c R^2 > (1/2q)$, we have $\lim_{\xi\to 1}(\partial A_p/\partial \xi) > 0$ the peak AoI A_p can then be optimized when $\xi \in (0, 1)$. By combining $(\partial A_p/\partial \xi) = 0$ and (5), the optimal packet arrival rate ξ can be obtained as

$$\xi = \frac{2q \exp\left\{-\frac{2}{\sqrt{1+\frac{4}{q\lambda c R^2}}+1} - \theta R^\alpha \gamma^{-1}\right\}}{q\lambda c R^2\left(\sqrt{1+\frac{4}{q\lambda c R^2}}+1\right) + 2q\exp\left\{-\frac{2}{\sqrt{1+\frac{4}{q\lambda c R^2}}+1} - \theta R^\alpha\gamma^{-1}\right\} - 2}. \tag{53}$$

The optimal peak AoI can be obtained by substituting (53) into (8).

When $\lambda c R^2 \le (1/2q)$, on the other hand, the optimal packet arrival rate is given by $\xi = 1$, and the corresponding optimal peak AoI can be obtained by combining $\xi = 1$ and (8).

APPENDIX G
PROOF OF THEOREM 4

We denote that

$$A_p^* = \min_{\{q\}} A_p^{\xi=\xi_q^*}. \tag{54}$$

From Theorem 3, for $q < (1/2\lambda c R^2)$, we have

$$\frac{\mathrm{d}A_p^{\xi=\xi_q^*}}{\mathrm{d}q} = \frac{2(\lambda c R^2 - \frac{1}{q})}{q} \exp\left\{\lambda c R^2 q + \theta R^\alpha \gamma^{-1}\right\}. \tag{55}$$

As $q < (1/2\lambda c R^2)$, thus, $(\mathrm{d}A_p^{\xi=\xi_q^*}/\mathrm{d}q) < 0$, which means that $A_p^{\xi=\xi_q^*}$ decrease monotonically when $q < (1/2\lambda c R^2)$. On the other hand, for $q > (1/2\lambda c R^2)$, we denote $k = -[2/\sqrt{1 + (4/q\lambda c R^2)} + 1]$, $k \in (-1, -[1/2])$, then

$$A_p^{\xi=\xi_q^*} = \frac{1}{\lambda c R^2 k^2 e^k e^{-\theta R^\alpha \gamma^{-1}}}. \tag{56}$$

We find that k decreases with the increase of q, $(1/e^k k^2)$ increases with the increase of k when $k \in (-1, -[1/2])$ and $(1/e^k k^2) > 0$, so $A_p^{\xi=\xi_q^*}$ decrease monotonically with the increase of q when $q > (1/2\lambda c R^2)$.

Moreover, when $\lambda c R^2 = (1/2q)$, $A_p^{\xi_q^*=1} = A_p^{\xi_q^*<1}$, which means $A_p^{\xi=\xi_q^*}$ is a continuous function for q, thus $A_p^{\xi=\xi_q^*}$ decrease monotonically for $q \in (0, 1]$.

Therefore, $A_p^* = A_p^{\xi=\xi_q^*}$ when $q = 1$ and Theorem 4 can be obtained by combining $q = 1$ and Theorem 3.

ACKNOWLEDGMENT

Any opinions, findings, and conclusions or recommendations expressed in this material are those of the author(s) and do not reflect the views of the National Research Foundation, Singapore, and Infocomm Media Development Authority.

REFERENCES

[1] D. Ciuonzo, P. S. Rossi, and P. K. Varshney, "Distributed detection in wireless sensor networks under multiplicative fading via generalized score tests," *IEEE Internet Things J.*, vol. 8, no. 11, pp. 9059–9071, Jun. 2021.

[2] D. Ciuonzo, P. S. Rossi, and P. Willett, "Generalized rao test for decentralized detection of an uncooperative target," *IEEE Signal Process. Lett.*, vol. 24, no. 5, pp. 678–682, May 2017.

[3] S. Kaul, R. Yates, and M. Gruteser, "Real-time status: How often should one update?" in *Proc. IEEE INFOCOM*, Orlando, FL, USA, Mar. 2012, pp. 2731–2735.

[4] R. D. Yates and S. Kaul, "Real-time status updating: Multiple sources," in *Proc. IEEE Int. Symp. Inf. Theory (ISIT)*, Cambridge, MA, USA, Jul. 2012, pp. 2666–2670.

[5] M. Costa, M. Codreanu, and A. Ephremides, "On the age of information in status update systems with packet management," *IEEE Trans. Inf. Theory*, vol. 62, no. 4, pp. 1897–1910, Apr. 2016.

[6] C. Kam, S. Kompella, G. D. Nguyen, J. E. Wieselthier, and A. Ephremides, "Controlling the age of information: Buffer size, deadline, and packet replacement," in *Proc. IEEE MILCOM*, Baltimore, MD, USA, Nov. 2016, pp. 301–306.

[7] R. Talak, S. Karaman, and E. Modiano, "Optimizing information freshness in wireless networks under general interference constraints," *IEEE/ACM Trans. Netw.*, vol. 28, no. 1, pp. 15–28, Feb. 2020.

[8] Q. He, D. Yuan, and A. Ephremides, "Optimizing freshness of information: On minimum age link scheduling in wireless systems," in *Proc. Int. Symp. Model. Optim. Mobile, Ad Hoc, Wireless Netw. (WiOpt)*, Tempe, AZ, USA, May 2016, pp. 1–8.

[9] I. Kadota, A. Sinha, E. Uysal-Biyikoglu, R. Singh, and E. Modiano, "Scheduling policies for minimizing age of information in broadcast wireless networks," *IEEE/ACM Trans. Netw.*, vol. 26, no. 6, pp. 2637–2650, Dec. 2018.

[10] I. Kadota and E. Modiano, "Minimizing the age of information in wireless networks with stochastic arrivals," *IEEE Trans. Mobile Comput.*, vol. 20, no. 3, pp. 1173–1185, Mar. 2021.

[11] B. Zhou and W. Saad, "Joint status sampling and updating for minimizing age of information in the Internet of Things," *IEEE Trans. Commun.*, vol. 67, no. 11, pp. 7468–7482, Nov. 2019.

[12] R. D. Yates and S. K. Kaul, "Status updates over unreliable multiaccess channels," in *Proc. IEEE Int. Symp. Inf. Theory (ISIT)*, Aachen, Germany, Jun. 2017, pp. 331–335.

[13] H. Chen, Y. Gu, and S.-C. Liew, "Age-of-information dependent random access for massive IoT networks," in *Proc. IEEE INFOCOM Workshop*, Toronto, ON, Canada, Jul. 2020, pp. 930–935.

[14] O. T. Yavascan and E. Uysal, "Analysis of slotted ALOHA with an age threshold," *IEEE J. Sel. Areas Commun.*, vol. 39, no. 5, pp. 1456–1470, May 2021.

[15] X. Chen, K. Gatsis, H. Hassani, and S. S. Bidokhti, "Age of information in random access channels," in *Proc. IEEE Int. Symp. Inf. Theory (ISIT)*, Los Angeles, CA, USA, Jun. 2020, pp. 1770–1775.

[16] J. Sun, Z. Jiang, B. Krishnamachari, S. Zhou, and Z. Niu, "Closed-form Whittle's index-enabled random access for timely status update," *IEEE Trans. Commun.*, vol. 68, no. 3, pp. 1538–1551, Mar. 2020.

[17] H. ElSawy, A. Sultan-Salem, M. Alouini, and M. Z. Win, "Modeling and analysis of cellular networks using stochastic geometry: A tutorial," *IEEE Commun. Surveys Tuts.*, vol. 19, no. 1, pp. 167–203, 1st Quart., 2017.

[18] J. G. Andrews, A. K. Gupta, and H. S. Dhillon, "A primer on cellular network analysis using stochastic geometry," 2016. [Online]. Available: arXiv:1604.03183.

[19] Y. Hu, Y. Zhong, and W. Zhang, "Age of information in Poisson networks," in *Proc. Int. Conf. Wireless Commun. Signal Process. (WCSP)*, Hangzhou, China, Oct. 2018, pp. 1–6.

[20] H. H. Yang, A. Arafa, T. Q. S. Quek, and H. V. Poor, "Optimizing information freshness in wireless networks: A stochastic geometry approach," *IEEE Trans. Mobile Comput.*, vol. 20, no. 6, pp. 2269–2280, Jun. 2021.

[21] M. Emara, H. Elsawy, and G. Bauch, "A spatiotemporal model for peak AoI in uplink IoT networks: Time versus event-triggered traffic," *IEEE Internet Things J.*, vol. 7, no. 8, pp. 6762–6777, Aug. 2020.

[22] H. H. Yang, A. Arafa, T. Q. S. Quek, and H. V. Poor, "Age of information in random access networks: A spatiotemporal study," in *Proc. IEEE Global Commun. Conf. (GLOBECOM)*, Taipei, Taiwan, Dec. 2020, pp. 1–6.

[23] H. H. Yang, C. Xu, X. Wang, D. Feng, and T. Q. S. Quek, "Understanding age of information in large-scale wireless networks," *IEEE Trans. Wireless Commun.*, vol. 20, no. 5, pp. 3196–3210, May 2021.

[24] P. D. Mankar, Z. Chen, M. A. Abd-Elmagid, N. Pappas, and H. S. Dhillon, "Throughput and age of information in a cellular-based IoT network," *IEEE Trans. Wireless Commun.*, early access, Jun. 29, 2021, doi: 10.1109/TWC.2021.3091540.

[25] P. D. Mankar, M. A. Abd-Elmagid, and H. S. Dhillon, "Spatial distribution of the mean peak age of information in wireless networks," *IEEE Trans. Wireless Commun.*, vol. 20, no. 7, pp. 4465–4479, Jul. 2021.

[26] F. Baccelli and B. Blaszczyszyn, *Stochastic Geometry and Wireless Networks: Volume I Theory*. Boston, MA, USA: Now Found. Trends, 2009.

[27] K. Stamatiou and M. Haenggi, "Random-access Poisson networks: Stability and delay," *IEEE Commun. Lett.*, vol. 14, no. 11, pp. 1035–1037, Nov. 2010.

[28] V. Tripathi, R. Talak, and E. Modiano, "Age of information for discrete time queues," 2019. [Online]. Available: arXiv:1901.10463.

[29] L. Dai, "Stability and delay analysis of buffered aloha networks," *IEEE Trans. Wireless Commun.*, vol. 11, no. 8, pp. 2707–2719, Aug. 2012.

[30] *Smart Grid Traffic Behaviour Discussion*, document RAN WG2 Meeting #69b, 3GPP R2-102340, Verizon, New York, NY, USA, Apr. 2020.

[31] M. Haenggi, J. G. Andrews, F. Baccelli, O. Dousse, and M. Franceschetti, "Stochastic geometry and random graphs for the analysis and design of wireless networks," *IEEE J. Sel. Areas Commun.*, vol. 27, no. 7, pp. 1029–1046, Sep. 2009.

Xinghua Sun (Member, IEEE) received the Ph.D. degree from the City University of Hong Kong (CityU), Hong Kong, in 2013.

In 2010, he was a visiting student with INRIA, Bordeaux, France. In 2013, he was a Postdoctoral Fellow with CityU. From 2015 to 2016, he was a Postdoctoral Fellow with the University of British Columbia, Vancouver, BC, Canada. From July to August 2019, he was a Visiting Scholar with Singapore University of Technology and Design, Singapore. From 2014 to 2018, he was an Associate Professor with Nanjing University of Posts and Telecommunications, Nanjing, China. Since 2018, he has been an Associate Professor with Sun Yat-sen University, Guangzhou, China. His research interests are in the area of stochastic modeling of wireless networks and machine learning over networks.

Dr. Sun served as the Technical Program Committee Member for numerous IEEE conferences.

Fangming Zhao received the B.E. degree in communication engineering from the School of Information Engineering, Guangdong University of Technology, Guangzhou, China, in 2019. He is currently pursuing the M.E. degree in information and communication engineering with the School of Electronics and Communication Engineering, Sun Yat-sen University (Shenzhen Campus), Shenzhen, China.

His research interests include age of information, queueing theory, and stochastic modeling of wireless network.

Howard H. Yang (Member, IEEE) received the B.E. degree in communication engineering from Harbin Institute of Technology, Harbin, China, in 2012, the M.Sc. degree in electronic engineering from Hong Kong University of Science and Technology, Hong Kong, in 2013, and the Ph.D. degree in electrical engineering from Singapore University of Technology and Design (SUTD), Singapore, in 2017.

He was a Postdoctoral Research Fellow with SUTD from 2017 to 2020, a Visiting Postdoctoral Researcher with Princeton University, Princeton, NJ, USA, from 2018 to 2019, and a visiting student with the University of Texas at Austin, Austin, TX, USA, from 2015 to 2016. He is currently an Assistant Professor with the Zhejiang University/University of Illinois at Urbana–Champaign Institute (ZJU-UIUC Institute), Zhejiang University, Haining, China. He is also an Adjunct Assistant Professor with the Department of Electrical and Computer Engineering, University of Illinois at Urbana–Champaign, Champaign, IL, USA. His research interests cover various aspects of wireless communications, networking, and signal processing, currently focusing on the modeling of modern wireless networks, high-dimensional statistics, graph signal processing, and machine learning.

Dr. Yang received the IEEE WCSP 10-Year Anniversary Excellent Paper Award in 2019 and the IEEE WCSP Best Paper Award in 2014.

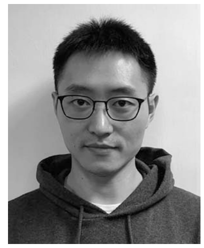

Wen Zhan (Member, IEEE) received the B.S. and M.S. degrees from the University of Electronic Science and Technology of China, Chengdu, China, in 2012 and 2015, respectively, and the Ph.D. degree from the City University of Hong Kong, Hong Kong, in 2019.

He was a Research Assistant and a Postdoctoral Fellow with the City University of Hong Kong. Since 2020, he has been with the School of Electronics and Communication Engineering, Sun Yat-sen University, Guangzhou, China, where he is currently an Assistant Professor. His research interests include Internet of Things, modeling, and performance optimization of next-generation mobile communication systems.

Xijun Wang (Member, IEEE) received the B.S. degree (with Highest Hons.) in communications engineering from Xidian University, Xi'an, China, in 2005, and the Ph.D. degree in electronic engineering from Tsinghua University, Beijing, China, in January 2012.

He was an Assistant Professor from 2012 to 2015 and an Associate Professor from 2015 to 2018 with the School of Telecommunications Engineering, Xidian University. From 2015 to 2016, he was a Postdoctoral Research Fellow with the Information Systems Technology and Design Pillar, Singapore University of Technology and Design, Singapore. He is currently an Associate Professor with Sun Yat-sen University, Guangzhou, China. His current research interests include age of information, edge computing, and IoT.

Dr. Wang was a recipient of the Best Paper Award from the IEEE ICCC 2013. He was recognized as an Exemplary Reviewer of the IEEE Wireless Communications Letters in 2014.

Tony Q. S. Quek (Fellow, IEEE) received the B.E. and M.E. degrees in electrical and electronics engineering from Tokyo Institute of Technology, Tokyo, Japan, in 1998 and 2000, respectively, and the Ph.D. degree in electrical engineering and computer science from the Massachusetts Institute of Technology, Cambridge, MA, USA, in 2008.

He is currently the Cheng Tsang Man Chair Professor with Singapore University of Technology and Design (SUTD), Singapore. He also serves as the Director of the Future Communications Research and Development Programme, the Head of ISTD Pillar, and the Deputy Director of the SUTD-ZJU IDEA, Singapore. His current research topics include wireless communications and networking, network intelligence, Internet of Things, URLLC, and big data processing.

Dr. Quek was honored with the 2008 Philip Yeo Prize for Outstanding Achievement in Research, the 2012 IEEE William R. Bennett Prize, the 2015 SUTD Outstanding Education Awards—Excellence in Research, the 2016 IEEE Signal Processing Society Young Author Best Paper Award, the 2017 CTTC Early Achievement Award, the 2017 IEEE ComSoc AP Outstanding Paper Award, the 2020 IEEE Communications Society Young Author Best Paper Award, the 2020 IEEE Stephen O. Rice Prize, the 2020 Nokia Visiting Professor, and the 2016–2020 Clarivate Analytics Highly Cited Researcher. He is a Distinguished Lecturer of the IEEE Communications Society. He has been actively involved in organizing and chairing sessions, and has served as a member of the Technical Program Committee as well as a symposium chair in a number of international conferences. He is currently serving as an Editor for the IEEE Transactions on Wireless Communications and an Elected Member of the IEEE Signal Processing Society SPCOM Technical Committee. He was an Executive Editorial Committee Member for the IEEE Transactions on Wireless Communications and an Editor for the IEEE Transactions on Communications and the IEEE Wireless Communications Letters.